J Herbmed Pharmacol. 2024; 13(4): 659-673.

http://www.herbmedpharmacol.com doi: 10.34172/jhp.2024.52606

Journal of Herbmed Pharmacology

Unveiling neuroprotective mechanisms of diosgenin and pterostilbene in diabetes-associated Alzheimer's disease through multi-target molecular docking approach

Syeda Jabeen Fatima[1], **Devarakonda Krishna Prasad**[1*]

[1]Department of Pharmacology, Anurag University, Venkatapur, Ghatkesar Rd., Hyderabad, 500088, Telangana, India

ARTICLE INFO

Article Type:
Original Article

Article History:
Received: 13 June 2024
Accepted: 27 August 2024
epublished: 1 October 2024

Keywords:
Alzheimer's disease
Diabetes mellitus
Diosgenin
Molecular docking
Pterostilbene

ABSTRACT

Introduction: Diabetes mellitus (DM) and Alzheimer's disease (AD) are two highly linked disorders due to their association with the aging population. Several studies have reported the beneficial effects of diosgenin and pterostilbene in treating neurodegenerative diseases. This study aimed to investigate the neuroprotective mechanisms of diosgenin and pterostilbene through molecular docking and dynamics studies and assess their pharmacokinetic parameters.

Methods: To understand the link between diabetes and AD, molecular docking of the natural ligands diosgenin and pterostilbene against the specific targets of AD, including β-secretase, glycogen synthetase kinase beta (GSK-3β), gamma-secretase, tumor necrosis factor-alpha (TNF-α), and interleukin-6 (IL-6) was done to find out their binding affinities to explain the molecular mechanisms involved in their neuroprotection. Further molecular dynamics studies and binding energy calculations for the ligands with GSK-3β and β-secretase were carried out to confirm their docking activities. Additionally, pharmacokinetic analysis of these two phytoconstituents was performed by the SWISSADME server.

Results: Molecular docking and dynamics studies revealed the good docking activity of diosgenin and pterostilbene with the selected targets. Further, the two phytoconstituents revealed suitable pharmacokinetic parameters along with blood-brain barrier permeability, confirming their druggable nature.

Conclusion: This research identified multiple neuroprotective pathways of diosgenin and pterostilbene that might be significant for treating diabetes-associated Alzheimer's disease.

Implication for health policy/practice/research/medical education:
Implications for health policy/practice/research/medical education: This article elucidated the multiple molecular mechanisms by which diosgenin and pterostilbene interacted with specific targets to provide neuroprotection in diabetes-induced Alzheimer's patients, opening new pathways for further research. This work may introduce new drug candidates with enhanced therapeutic efficacy, reduced cost, easy accessibility, and fewer side effects than conventional medications.

Please cite this paper as: Fatima SJ, Prasad DK. Unveiling neuroprotective mechanisms of diosgenin and pterostilbene in diabetes-associated Alzheimer's disease through multi-target molecular docking approach. J Herbmed Pharmacol. 2024;13(4):659-673. doi: 10.34172/jhp.2024.52606.

Introduction

Diabetes mellitus (DM) and Alzheimer's disease (AD), the two highly linked disorders have been identified as the greatest threats in the history of medical sciences. DM is the most prevalent endocrine disorder, with an estimated 415 million people suffering from it worldwide (1). AD is a common neurodegenerative disorder affecting 50 million people globally with reports expecting it to be doubled by 2030, according to World Alzheimer Disease Report (2). Evidence suggests a strong epidemiological and pathophysiological association between DM and AD, as the two share common pathogenic pathways such as persistent hyperglycemia, beta-amyloid deposition in the tissues, and oxidative stress leading to toxicity and inflammation (3). Chronic diabetes is implicated in cognitive decline, including attention dysfunction,

***Corresponding author**: Devarakonda Krishna Prasad,
Email: krishnaprasadpharmacy@anurag.edu.in

problems with learning and memory, and dementia. Thus, the term type 3 DM has often been used to describe AD-associated dementia caused by insufficient insulin receptor signaling and insulin resistance in the brain (4). AD involves progressive, irreversible memory loss with behavioral disturbance.

Deposition of beta-amyloid in brain parenchyma forms senile plaques as a result of proteolytic cleavage of amyloid precursor proteins by beta-secretase (β-secretase) and gamma-secretase (γ-secretase); the aberrant tau hyperphosphorylation by glycogen synthetase kinase beta (GSK-3β) resulting in neurofibrillary tangles are the main characteristics of AD. Due to these inclusions causing synaptic loss, oxidative stress, and neuroinflammation, particularly in the neocortex and hippocampus, neuronal dysfunction occurs leading to decreased levels of acetylcholine (ACh) (5). This hypothesis explains the use of AChE inhibitors like donepezil, rivastigmine, and galantamine in the therapy of AD to increase ACh levels by preventing its metabolism (6). However, none of these drugs has proven to totally stop the disease progression. Elevated AChE levels and poor glycemic control trigger chronic inflammatory processes in the brain, resulting in damaged neurons due to microglial activation releasing inflammatory cytokines such as interleukin-6 (IL-6) and tumor necrosis factor-alpha (TNF-α) (7). With AD being regarded as a complex disorder involving multiple molecular targets, the usual one-target one-drug approach might not be an effective strategy in its drug development. Instead, a drug capable of acting simultaneously on different targets may be a more promising approach (8,9). Although there is evidence for a strong association between DM and AD, the exact pathological mechanism linking the two disorders remains unknown. Therefore, we aim to identify the linking molecular pathways by screening the common pharmacological targets, which may provide newer therapeutic options in the treatment of DM and AD.

Natural compounds have long been relied on to manage various disorders due to the presence of a wide range of bioactive substances demonstrating potential therapeutic benefits (10). Diosgenin obtained from *Dioscorea* species, is a natural steroidal saponin with effects similar to phytoestrogens. Multiple biological effects of diosgenin have been reported, including anti-hyperglycemic, cardioprotective, anti-hyperlipidemic, anti-inflammatory, and antioxidant effects (11). It also enhanced spatial learning and memory in animals with amyloid-beta-peptide-induced cognitive deficits (12). Pterostilbene, obtained from *Pterocarpus marsupium*, also demonstrated various activities like anti-inflammatory, antioxidant, anticancer, and neuroprotection (13). Pterostilbene was also reported to improve the amyloid beta-induced neuroplastic inflammation in mice (14). Diosgenin and pterostilbene were selected for the study because of their encouraging therapeutic potential as antioxidants and anti-inflammatory agents. Being natural plant-based products, they are less expensive alternatives with fewer side effects (14). However, the underlying neuroprotective mechanisms of both phyto-molecules were yet to be discovered.

Recent developments have identified enzymes as the most promising therapeutic targets involved in the pathogenesis of various diseases. GSK-3β, β-secretase, γ-secretase, TNF-α, and IL-6 were selected as common interlinking target proteins for molecular docking, associated both with diabetes and AD. This study performed molecular docking, molecular dynamic (MD) simulation studies, free energy computation, and pharmacokinetic evaluation for the ligand's diosgenin and pterostilbene to identify the therapeutically active molecular pathways. The anticipated outcome of this investigation is to introduce a novel combination against diabetes-associated AD treatment through multiple enzyme target effects.

Methods

The workflow in this study comprised selecting and preparing protein targets and ligands for molecular docking, calculating binding free energy, simulating MD, and assessing pharmacokinetics. The 3D structures of target enzymes and ligands were identified and downloaded using the DrugBank and RCSB-PDB databases (http://www.rcsb.org/pdb/).

Molecular docking

The docking study selected GSK-3β (PDB:1J1B, Resolution: 1.8 Å), β-secretase (PDB:1TQF, Resolution: 1.8 Å), γ-secretase (PDB:6IYC, Resolution: 2.6 Å), TNF-α (PDB:5M2J, Resolution: 1.9 Å), and IL-6 (PDB:1ALU, Resolution: 1.9 Å) x-ray crystal structures for docking. Schrödinger 2019-2's protein preparation wizard module was used for protein preparation (15). Crystallographic water molecules were eliminated by hydrogen addition. Prime (Schrödinger 2019-2) was used to incorporate the missing side chains (16). Root mean square deviations (RMSDs) of heavy atoms were maintained at 0.30 Å using the OPLS3e forcefield for energy reduction (17). A 10 Å radius surrounding the bound ligand defined the active site, and a grid box was created with the co-crystallized ligand at its core. The docking protocol was validated using the extra precision (XP) Glide docking procedure employing redocking protocol, where the co-crystal ligands from the binding sites of human tau protein kinase, GSK-3β (PDB:1J1B) and β-secretase (PDB:1TQF) were removed and redocked in their respective binding sites. The two ligands, pterostilbene and diosgenin (Figure 1), were synthesized using LigPrep and docked with Glide in the extra-precision (XP) mode, leaving other options default (18). The ligand's ideal docking location was chosen based on the values of the docking score, glide energy, and glide Emodel energy.

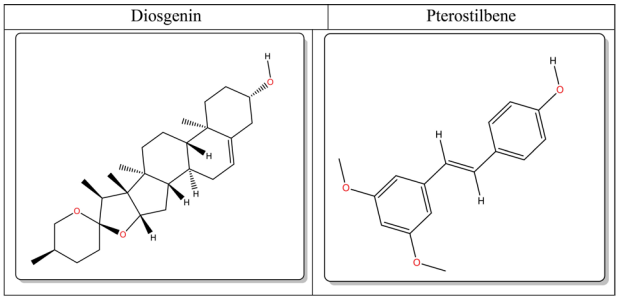

Figure 1. Chemical structures of the two selected ligands, diosgenin and pterostilbene.

Molecular dynamics simulation

Using the Desmond software, the docked complex of diosgenin and pterostilbene in complex with 1TQF (GSK-3β) and 1J1B (β-secretase), was chosen to run the MD simulation with the OPLS3e force feld (Schrödinger 2019-2). When the molecular system was solvated with TIP4P water molecules, the protein and the borders of the orthorhombic box were approximately 10 Å apart. In order to neutralize the system, the proper counter Na+ ions were introduced. To minimize the solvated system using limited memory, three vectors and ten steepest descent steps were employed, until the gradient threshold of 25 kcal/mol/Å was reached (Broyden-Fletcher-Goldfarb-Shanno) (19). The Ewald approach was utilized for distant electrostatic interactions with smooth particle mesh at a tolerance of 1e−09 and for short-range columbic interactions with a radius of cut-off of 9.0 Å (20). The temperature was maintained at 300 k and the pressure at 1 bar using the Nose-Hoover thermostat and the Martyna-Tobias-Klein barostat, respectively (21,22). The time step chosen was 2 fs to simulate the molecular system for 100 ns under isothermal-isobaric ensemble (NPT) conditions. Frames were built every 100 ps using a REPSA integration algorithm with multiple time steps for interactions that are bound, distant from bonded, and close to non-bonded (2, 2, and 6 fs, respectively) (23). Trajectory posture and three-dimensional structure analysis were generated using the Maestro graphical user interface.

Binding free energy calculations

For each protein-ligand complex, the binding free energy was determined using the PRIME Molecular Mechanics-Generalized Born Surface Area (MM-GBSA) technique (Schrödinger 2019-2). The VSGB 2.0 solvation model, in conjunction with the OPLS3e force field, was utilized to minimize energy. This approach combines an optimized implicit solvation with a physics-based correction for hydrophobic interactions, self-contact interactions, π–π interactions, and hydrogen bonding (24).

Drug-likeness properties & ADMET analysis

Lipinski's rule of five (RO5) establishes a set of criteria for evaluating drug-likeness, a crucial parameter in the discovery of novel medications. These criteria include a molecular weight of less than 500 Da, a maximum of five hydrogen bond donors, a maximum of 10 hydrogen bond acceptors, and a value of AlogP of no more than five. The SwissADME server was used to check the bioavailability of diosgenin and pterostilbene and analyze various other rules (25-28). The server was also utilized to track the pharmacokinetic parameters, such as absorption, distribution, metabolism, and excretion, as well as toxicity, solubility, and some other pharmacokinetic factors (29). Selected ligands' SMILES were uploaded to the webserver to assess the various parameters.

Results

Various approaches used for *in silico* analysis:

1. Molecular docking of ligands (diosgenin and pterostilbene)
   - GSK-3β
   - β-Secretase
   - γ-Secretase
   - IL-6
   - TNF-α
2. Molecular dynamics (Diosgenin and Pterostilbene)
   - GSK-3β
   - β-Secretase
3. Binding free energy calculations
4. Drug-likeness properties and ADMET analysis

Molecular docking analysis

The docking protocol was validated based on its ability to reproduce the binding mode of the GSK-3β and β-secretase bound co-crystalized inhibitors, respectively. Similar orientation was observed between the conformations of XP docked pose and co-crystal pose with a low root mean square deviation (PDB:1J1B - RMSD: 1.51Å and PDB:1TQF - RMSD: 1.35Å) as shown in Figure 2. This suggests the reliability of our Glide XP-docking protocol in reproducing the experimentally observed binding modes of inhibitors. Molecular docking of the two ligands diosgenin and pterostilbene with the receptors GSK-3β (PDB:1J1B), β-secretase (PDB:1TQF), γ-secretase (PDB:6IYC), TNF-α (PDB:5M2J), and IL-6 (PDB:1ALU) revealed several interactions of the ligands and their docking scores, as represented in Table 1, confirming their proposed multitarget nature.

GSK-3β (PDB:1J1B) docking with diosgenin and pterostilbene

The homodimer GSK-3β crystal structure showed that each monomer was made up of a small N-terminal domain composed of beta sheets and a large C-terminal domain made up of loops and alpha helices. The most important ATP binding site, located at the interface of the alpha and beta helical strands, is formed by the catalytic domain and substrate binding site. Most interactions made at the ATP binding site are hydrophobic and polar. The hydroxyl group of diosgenin formed a hydrogen

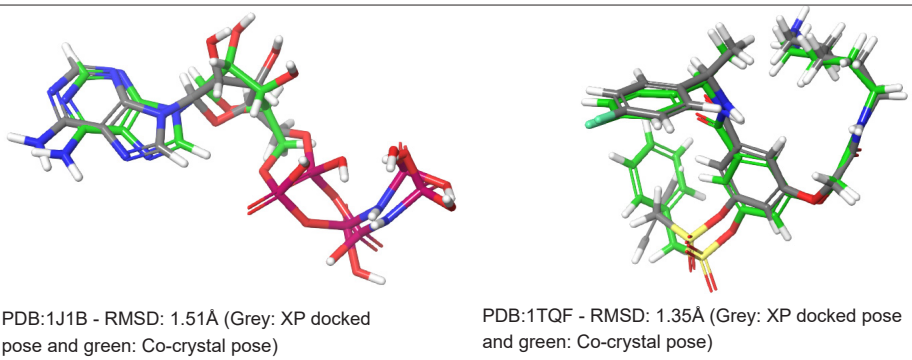

Figure 2. Comparison between the docked pose of the GSK3β and β-secretase inhibitors as produced by the docking study (grey) and the original crystallographic structure of the same inhibitor within the binding pockets (green).

bond with Ser66 (bond length 2.10Å) of the N-terminal, located near the substrate binding site. The hydrophobic interactions were shown with Val70, Phe67, Ile62, Ala83, Tyr134, Val135, Leu188, and Cys199 located in N and C terminal domains important for substrate recognition. Polar interactions were shown with Ser66, Asn64, Thr138, Gln185, Asn186 (Figure 3a). Interactions with Thr138 and Gln185 play a role in the complex binding stabilization. Docking with pterostilbene showed two hydrogen bonds formed between the hydroxyl group at the phenyl ring with the -NH backbone of Val135 (bond length 2.17Å) and Asp133 (bond length 2.08Å). In the ATP binding domain, the hydrophobic pocket was formed with Val110, Leu132, Ala83, Tyr134, Val135, Cys199, Val70, Phe67, Ile62, and Leu188 and polar interactions with Asn186, Gln185, Ser66 and Asn64 (Figure 4a). The docking scores of diosgenin and pterostilbene, with GSK-3β were found to be -9.25 kcal/mol and -10.99 kcal/mol, respectively.

β-Secretase (PDB:1TQF) docking with diosgenin and pterostilbene

The 3D crystal structure of the beta-site amyloid precursor protein cleaving enzyme is structurally a challenging protein with multiple sites showing effective binding. It shows eleven pockets, an essential feature influencing the interaction with ligands, having several sub-pockets, such as S1, S2, S21, S3, S31, S4, and S41, with binding mostly in S2-S21 and S3-S21. Figure 3b and Figure 4b respectively show the interaction of the ligands diosgenin and pterostilbene with the β-secretase enzyme. Ligand diosgenin contacts the residues Ile110, Leu30 and Trp115 in the S3 pocket and has polar interactions with Gln326, Ser325, Asn233, Thr232, Thr231, Gln12, Thr72 and Gln73 in the S2 pocket. The ligand pterostilbene shows two hydrogen bonds with its hydroxyl group with Ser325 (bond length 3.12Å) and its methoxy group with Asp32 in the S1 pocket. It also showed hydrophobic interactions with Tyr71, Phe108, Trp115, Ile118, Leu30 in the S1 pocket and polar interactions with Ser325, Gln73, Thr72, Asn233, Thr232, Thr231, and Ser35 in the S1 and S2 pockets. The docking score of diosgenin and pterostilbene with β-secretase was found to be -7.67 kcal/mol and -8.56 kcal/mol, respectively.

γ-Secretase (PDB:6IYC) docking with diosgenin and pterostilbene

Human γ-secretase X-ray crystal structures disclose the four main subunits comprising presenilin (PS), PEN-2 (presenilin enhancer-2), APH-1 (anterior pharynx defective-1), and nicastrin. The catalytic part, presenilin, and the two transmembrane aspartates within the active site of the membrane-embedded protease complex are mainly responsible for their action. Presenilin (PS1) is formed of transmembrane helices with residues at their interface responsible for their inhibition. Binding in diosgenin is primarily due to hydrophobic interactions with Val138 and Cys140 and polar interactions with His158, Gln163, and Gln139 residues (Figure 3c). Pterostilbene has a pair of hydrogen bonds with its hydroxy group and N backbone of the amino acids Asn55 (bond length 2.77Å) and Asp336 (bond length 1.58Å), with many hydrophobic interactions shown with Trp648, Tyr173, Phe145, Cys140, and Val138. It also showed few polar interactions with Asn55, Gln139, and His158 residues (Figure 4c). The docking scores of

Table 1. Docking scores of diosgenin and pterostilbene in complex with various proteins

S. No.	Ligand	Docking score (kcal/mol)				
		GSK-3β	β-secretase	γ-secretase	IL-6	TNF-α
1.	Diosgenin	-9.254	-7.679	-8.578	-2.329	-3.631
2.	Pterostilbene	-10.995	-8.561	-9.869	-5.528	-4.611

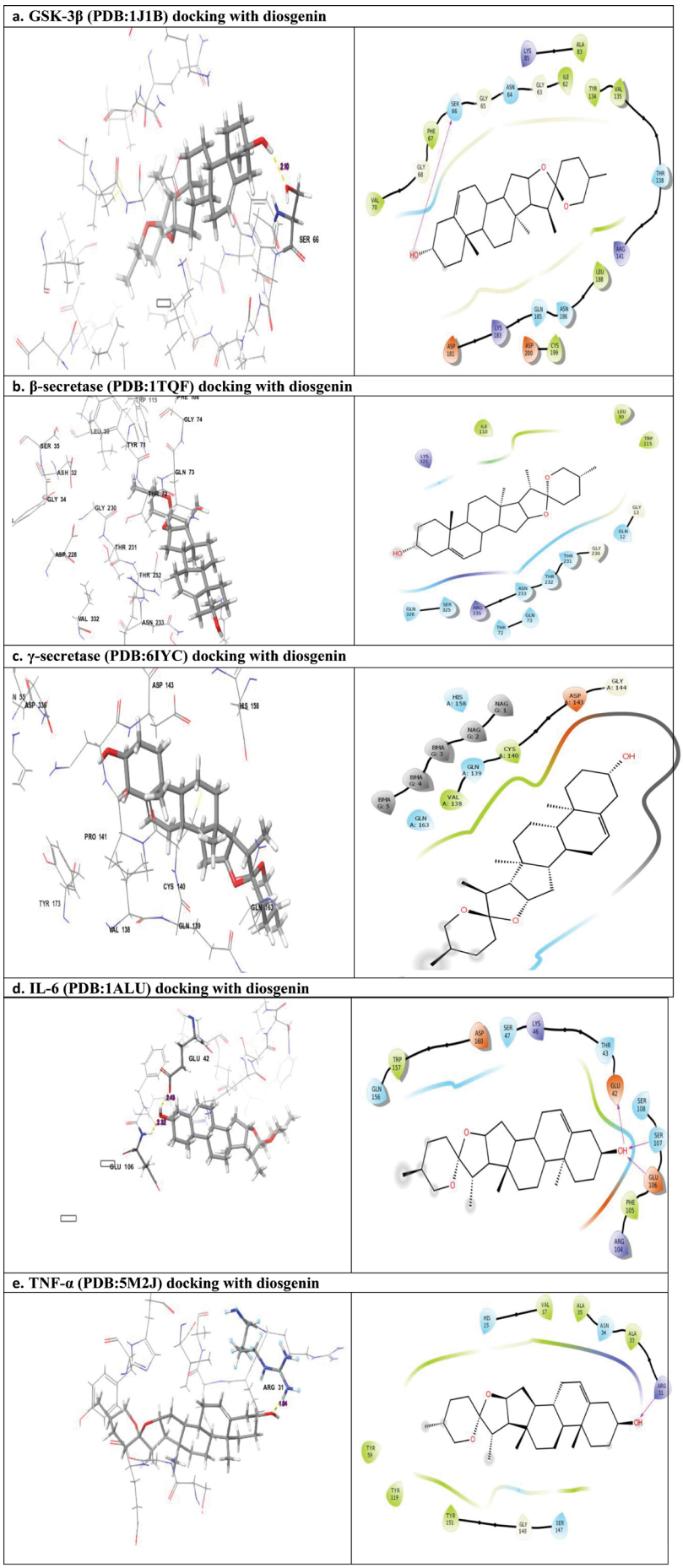

Figure 3. Molecular interactions of diosgenin with various targets. The hydrogen bond contacts and residues are indicated by a yellow-dotted line, while the pink numbers represent their distances in the first image. The 2D image represents the types of contacts formed between the ligand and receptor protein indicated by various colors: with green color "hydrophobic bond", blue color "polar bond", red color "charged -ve residue", purple color "charged +ve residue", grey color "metal or unspecified residue", purple arrow "hydrogen bond", yellow arrow "halogen bond", red line with a dot "pi cation interaction", green line with dots "pi-pi stacking", and a multicolored line "salt bridge".

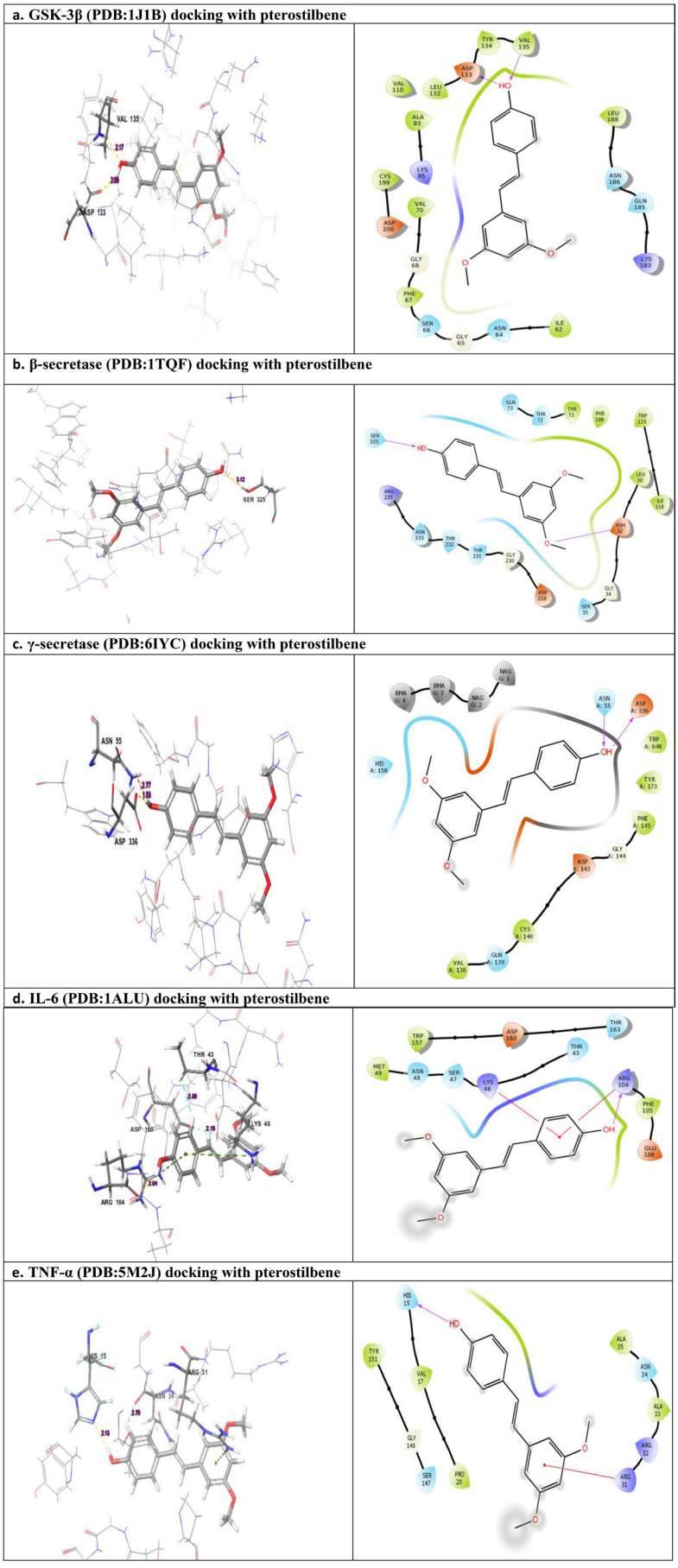

Figure 4. Molecular interactions of pterostilbene with various targets. The hydrogen bond contacts and residues are indicated by a yellow dotted line, while the pink numbers represent their distances in first image. The 2D image represents the types of contacts formed between the ligand and receptor protein indicated by various colors: with green color "hydrophobic bond", blue color "polar bond", red color "charged -ve residue", purple color "charged +ve residue", grey color "metal or unspecified residue", purple arrow "hydrogen bond", yellow arrow "halogen bond", red line with a dot "pi cation interaction", green line with dots "pi-pi stacking", and a multicolored line "salt bridge".

diosgenin and pterostilbene with γ-secretase were found to be -8.578 kcal/mol and -9.869 kcal/mol, respectively.

IL-6 (PDB:1ALU) docking with diosgenin and pterostilbene

Four interconnected helices A, B, C, and D, and an additional helix E in the long loop, comprise the crystal structure of IL-6. Molecular docking with the ligand diosgenin revealed three hydrogen bonds with its 3-hydroxyl group and Glu42 (bond length 2.43Å) on the A helix and Glu106 (bond length 2.32Å), Ser107 located on the brief cross-over link that unites the B and C helices. The hydrogen bonds formed play a crucial role in its inhibition upon binding. Furthermore, it showed hydrophobic interactions with Trp157 and Phe105 and polar interactions with Ser47, Thr43, Ser107, and Ser108. Docking with the ligand pterostilbene showed a hydrogen bond with its hydroxyl group and Arg104 (bond length 2.06Å) located on the connecting short crossover between B&C helices. Hydrophobic interactions were formed with Trp157, Met49, Phe105, and polar interactions with Asn48, Ser47, Thr43, and Thr163. Additionally, it displayed π-cation interactions with Lys46 and Arg104. The interactions shown by the ligands diosgenin and pterostilbene in Figure 3d and Figure 4d confirmed their ability to inhibit the inflammatory mechanisms mediated by IL-6.

TNF-α (PDB:5M2J) docking with diosgenin and pterostilbene

The crystallographic structure of TNF-α on docking with the ligand diosgenin showed one hydrogen bond with its hydroxyl group and the Arg31 residue (bond length 1.94Å) in the binding site. Binding of TNF-α with diosgenin mainly involved hydrophobic interactions with Tyr59, Tyr119, Tyr151, Val17, Ala35, Ala33, and polar interactions with His15, Asn34, and Ser147 in its catalytic site (Figure 3e). Molecular docking with the ligand pterostilbene disclosed a hydrogen bond with its hydroxyl group and the His15 residue (bond length 2.13Å). It also showed hydrophobic interactions with Tyr15, Val17, Pro20, Ala35, Ala33, and polar interactions with Asn34, His15, and Ser147 residues in the catalytic binding site of TNF-α (Figure 4e). The interactions of the ligands diosgenin and pterostilbene with TNF-α indicated their possibility to modulate the inflammatory mechanisms to provide neuroprotection.

MD simulation analysis

To verify the dynamic behaviour and stability of 1J1B (GSK-3β) and 1TQF (β-secretase) bound with the ligands diosgenin and pterostilbene, the retrieved posture complexes were put through Desmond 100 ns MD simulations, incorporated with Schrodinger suite 2019-2. The root-mean-square deviation (RMSD) metrics for Cα (backbone carbon atoms in amino acids), the backbone, and the heavy atoms of the protein and ligand are shown in Figure 5 based on a detailed examination of the trajectory frames.

1J1B (GSK-3β) - Diosgenin simulation

The solvated system comprises of 19966 water molecules and 65678 atoms. After analysing the trajectory frames, the RMSD for the Cα, backbone, and ligand fit protein were found to be between 2.28 and 3.19, 1.52 and 2.83, and 0.28 and 3.24Å, respectively. The Cα RMSDs and inhibitor backbone combination increased until 13 ns during the equilibrium phase, and after 20 ns, they converged. Throughout 10-25 ns, variations in the Cα atoms RMSD values were noted with the 2.28–3.19Å range. The RMSD of the Cα atoms stabilized in the range of 3.19-2.16Å during a period of 50–100 ns after the equilibration phase (Figure 5a). The RMSF plot reveals the Cα and the backbone of essential binding residues of amino acids in the catalytic site showing variations in RMSF values within the range of 0.58-3.24 and 0.62-3.28Å, respectively. In the course of MD simulation, the specified protein inhibitor complex was found to have a steady radius of gyration (rGyr) for its Cα and backbone atoms, indicating a limited level of structural flexibility of the protein. Furthermore, it is suggested that the effect of solvency has led to the inhibitor-protein complex exhibiting more flexible conformations (stabilization). Throughout the simulation, the ligand's RMSD showed conformational changes starting at 13 ns and stabilizing at 20 ns. Figure 5a (i) also reveals the binding pocket residues RMSD adjusting effectively with inhibitory movement. Interactions such as hydrogen bonds, as well as hydrophobic and water bridges were noted with the stable specific residues Asp181-Lys183, Leu132-Tyr134, Asp181-Lys183, and Gln185-Leu188. However, no contacts were seen in the Val135-Thr138 region. The other interacting residues showing low RMSF values were Ile62, Phe67, Val70, Ala83, and Leu132. The binding interactions revealed by the MD simulation trajectory analysis were consistent with XP docking. The 3-hydroxy group of diosgenin showed hydrogen bonds, one each with Lys183, Cys199, and through a water molecule with Ser66. It exhibited key hydrophobic interactions with Ile62, Phe67, Val70, Ala83, Leu132, Tyr134, and Leu188 (Figure 5b). Additionally, 100 frames were taken out of simulation trajectory files, and the clustered structure of diosgenin/1J1B was created with the trajectory clustering molecule (Schrodinger 2019-2). The structure that was generated by diosgenin showed a single hydrogen bond with Lys183 and mainly hydrophobic interactions with Val70, Ala83, Tyr134, and Leu188 residues which correspond well with the crucial interactions shown in the MD simulation's ligand interaction diagram, and the outcome secured in docking study (Figure 6a). After 13 ns of molecular simulation analysis, diosgenin showed an average radius of gyration (rGyr) of 4.73Å and an average RMSD of 0.38Å. The polar surface area (PSA) 51.8-

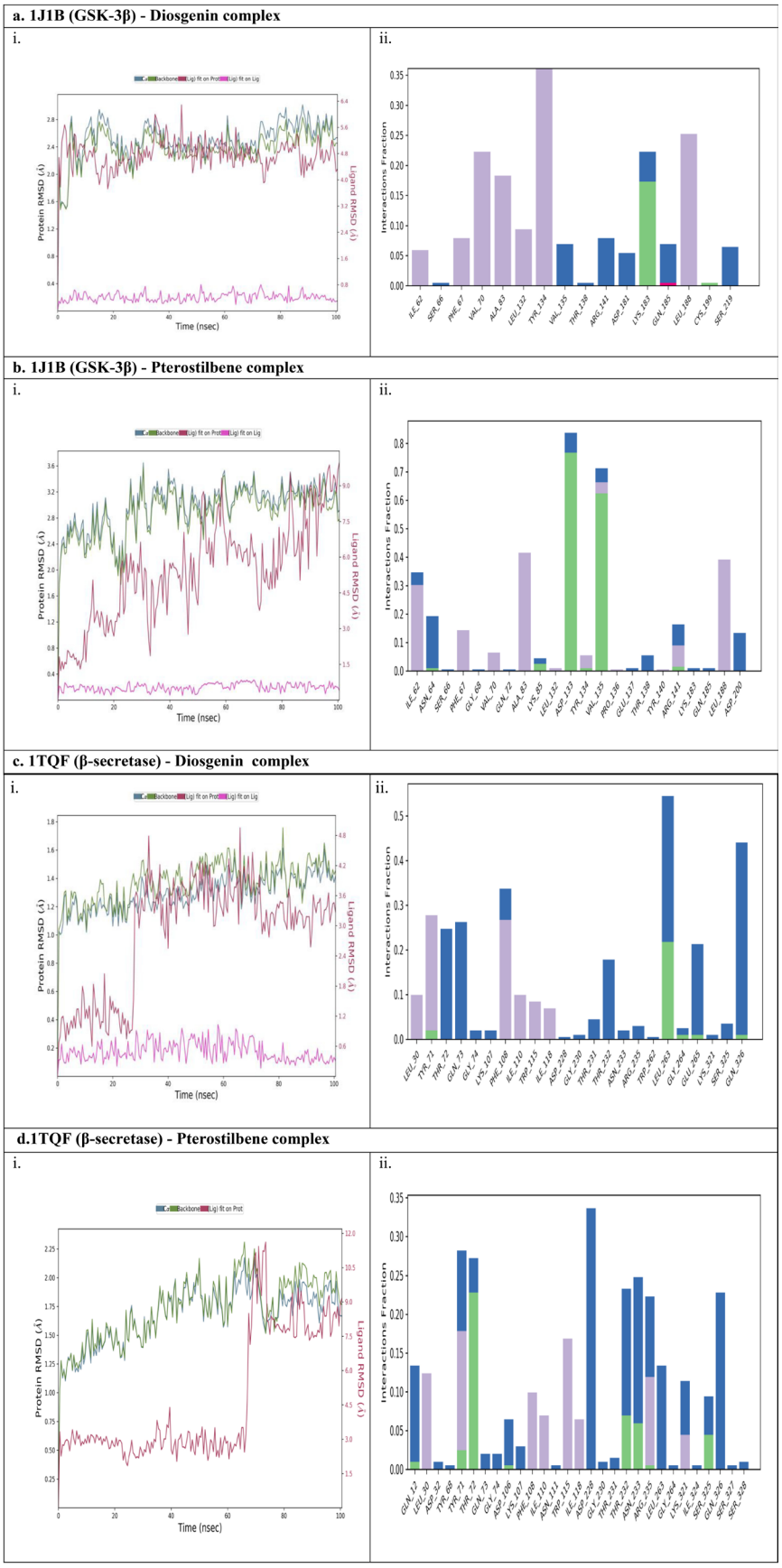

Figure 5. Molecular dynamics (MD) parameters change of various protein-ligand complexes. i. Root mean square deviations (RMSD) of the backbone atoms, Cα, and 1J1B simulated positions relative to the initial structure. ii. Illustrates the type of protein-ligand contacts with residues; green colour: hydrogen bonds; purple colour: hydrophobic bonds; pink colour: ionic; blue colour: water bridges.

61.4A^2 and stable solvent access area (SASA) 80.23-256A^2 demonstrated the stability of the inhibitor inside the binding pocket. Fewer molecular surface area (MolSA) changes of 378.61-387.23A^2 indicated the stability of diosgenin during the MD simulation study.

1J1B (GSK-3β) - Pterostilbene simulation

The solvated system comprises 19312 water molecules and 63787 atoms. Following the analysis of the trajectory frames, the Cα, backbone, and ligand fit protein RMSDs were determined to be between 2.42 and 3.71, 0.69 and 3.61, and 0.35 and 3.72 Å, respectively. The Cα RMSDs and inhibitor backbone combination increased until 30 ns during the equilibrium phase, and after 50 ns, they converged. Throughout 8–30 ns, variations in the Cα atoms RMSD values were noted in the 2.42–3.71Å range. The RMSD of the Cα atoms stabilized in the range of 3.71 and 2.97Å during 50 and 100 ns after the equilibration phase (Figure 5b). The RMSF plot revealed the Cα, backbone, and B factor of essential binding residues of amino acids in the catalytic site showing variations in RMSF values within the range of 0.66-4.09, 0.46-4.18 and 0.62-2.82Å, respectively (Figure 7b). In the course of MD simulation, the specified protein inhibitor complex was found to have a steady radius of gyration for its Cα and backbone atoms, indicating a limited level of structural flexibility of the protein. Furthermore, it is suggested that the effect of solvency has led to the inhibitor-protein complex exhibiting more flexible conformations (stabilization). Throughout the simulation, the ligand's RMSD showed conformational changes starting at 30 ns and stabilizing at 50 ns. Figure 5b (i) also reveals the binding pocket residues of RMSD adjusting effectively with inhibitory movement. Interactions such as hydrogen bonds and hydrophobic and water bridges were noted with the stable specific residues Leu132-Asp133, Tyr134-Val13, and Gln72-Ala83. However, no contacts were seen in Pro136-Glu137, Thr138-Tyr140, Arg141-Lys183, and Leu188-Asp200 regions. The other interacting residues showing low RMSF values were Ile62, Asn64, Phe67, Arg141, and Gln185. Binding interactions, shown by the MD simulation trajectory analysis, were in confirmation with the XP docking interactions. Similar binding interactions were shown by the MD simulation trajectory analysis as predicted by the XP docking interactions. The hydroxy group of the phenyl ring of pterostilbene showed two hydrogen bonds, one each with Asp133 and Val135 through a water molecule. These interactions occurred for more than 40% of the simulation time in the selected trajectory through 100 ns. It also exhibited key hydrophobic

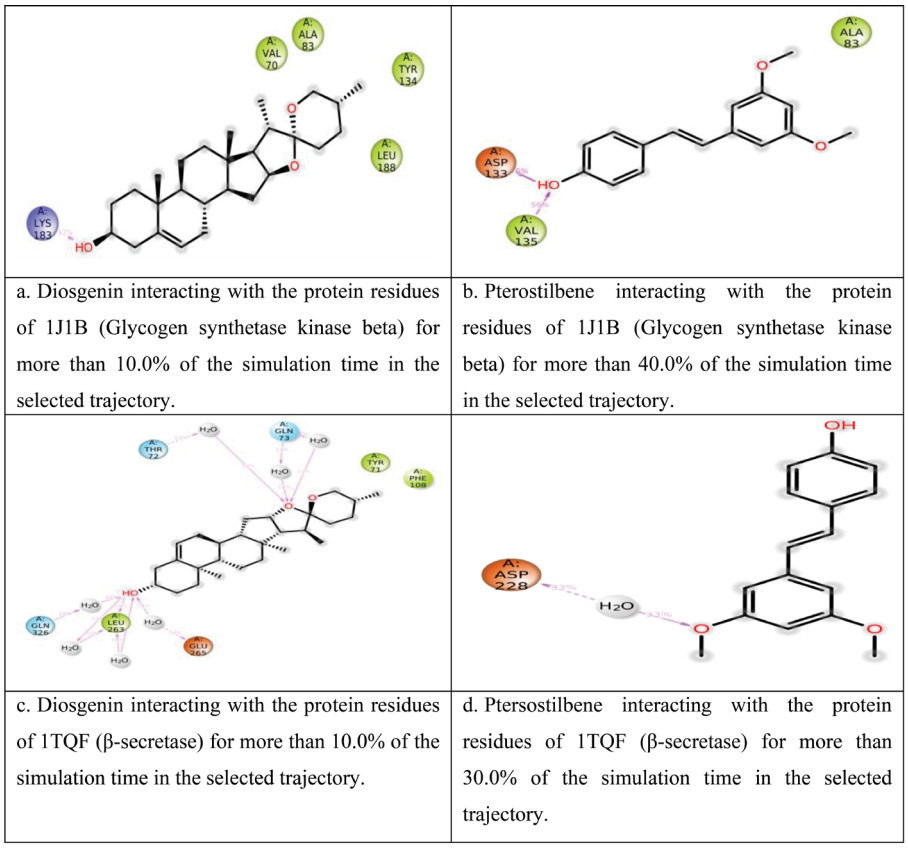

a. Diosgenin interacting with the protein residues of 1J1B (Glycogen synthetase kinase beta) for more than 10.0% of the simulation time in the selected trajectory.

b. Pterostilbene interacting with the protein residues of 1J1B (Glycogen synthetase kinase beta) for more than 40.0% of the simulation time in the selected trajectory.

c. Diosgenin interacting with the protein residues of 1TQF (β-secretase) for more than 10.0% of the simulation time in the selected trajectory.

d. Ptersostilbene interacting with the protein residues of 1TQF (β-secretase) for more than 30.0% of the simulation time in the selected trajectory.

Figure 6. Specific ligand-atom interactions with the protein residues. Interactions of the ligands with the protein residues of Glycogen synthetase kinase beta and β-secretase that take place in the chosen trajectory (0.00 through 100.50 nSec) are represented with the colors green and red for hydrophobic and negatively charged states, respectively. Arrows indicate the hydrogen bonds through water molecules.

interactions with Ala83 and Leu188. Val135 is considered to be a critical interacting residue available throughout the MD study (Figure 5b). The moderate flexibility of Ile62, Asn64, Lys85, Thr138, Arg141, and Asp200 is responsible for intermittent frequency hydrogen bonding interaction. The MD simulation study's findings are consistent with the docking results. Additionally, 100 frames were taken out of simulation trajectory files, and the clustered structure of pterostilbene/1J1B was created with the trajectory clustering molecule (Schrodinger 2019-2). The structure generating pterostilbene showed two hydrogen bond interactions with Asp133 and Val135 residues, which corresponded well with the crucial interactions shown in the MD simulation's ligand interaction diagram and the outcome secured in the docking study (Figure 6b). Therefore, it is clearly understood that Asp133 and Val135 are essential for the stability of the inhibitors in the catalytic pocket. Pterostilbene revealed an average radius gyration (rGyr) of 4.21Å and an average RMSD of 0.42Å after 30 ns of the MD study. The polar surface area of 77.2-84.3A^2 and stable solvent access area of 78.24-240.7A^2 demonstrated the stability of the inhibitor inside the binding pocket. Fewer molecular surface area changes of 267.5-274.3A^2 indicated the stability of pterostilbene during the MD simulation study.

1TQF (β-secretase) - Diosgenin simulation

The solvated system comprises 13 453 water molecules and 46 293 atoms. After analyzing the trajectory frames, the RMSDs for the Cα, backbone, and ligand fit protein were found to be between 1.08 and 1.46, 1.11 and 1.74, and 0.26 and 1.78Å, respectively. The Cα RMSDs and inhibitor backbone combination increased until 21 ns during the equilibrium phase, and after 32 ns, they converged. Fluctuations were observed in the range of 1.41-1.22Å during 32-100 ns (Figure 5c). The RMSF plot revealed the Cα and the backbone of essential binding residues of amino acids in the catalytic site showing variations in RMSF values within the range of 0.42-2.88 and 0.46-3.42Å respectively (Figure 7c). In the course of MD simulation, the specified protein inhibitor complex was found to have a steady radius of gyration for its Cα and backbone atoms, indicating a limited level of structural flexibility of the protein. Furthermore, it is suggested that the effect of solvency has led to the inhibitor-protein complex, exhibiting more flexible conformations (stabilization). Throughout the simulation, the ligand's RMSD showed conformational changes starting at 32 ns and stabilizing at 40 ns. Figure 5c (i) also reveals the binding pocket residues RMSD, adjusting effectively with inhibitory movement. The most significant hydrogen bond interactions were observed with the stable key residues Leu30-Tyr71, Trp262-Leu263, Leu263-Gly264, Gly264-Glu265, and Ser325-Gln326. However, no interactions were observed in the region of Gln12 and Gly13. Water can bridge with Thr72, Gln73, Gly74, Lys107, Asp228, Gly230, Thr232, Thr232, Asn233, Arg235, Lys321, and Ser325. The 3-hydroxy group of the phenyl ring of diosgenin showed three hydrogen bonds, one each with Gln326, Leu263, and Glu265 through a water molecule. Its methoxy group showed two hydrogen bonds with Thr72 and Gln73 through a water molecule. It also exhibited key hydrophobic interactions with Leu30, Tyr71, Phe108, Ile110, Trp115, and Ile118 (Figure 5c). The MD simulation study's findings were quite consistent with the docking results. Furthermore, the clustered structure of diosgenin/1TQF was generated using the trajectory clustering molecule after 100 frames were retrieved from simulation trajectory files (Schrodinger 2019-2). The structure generated showed five hydrogen bond interactions with Gln326, Leu263, Glu265, Thr72, and Gln73 residues, which were the critical interactions not visualized in the docking study, confirmed by the MD simulation's ligand interaction diagram (Figure 6c). After 32 ns of MD study, diosgenin showed an average radius of gyration of 4.72Å and an average RMSD of 0.42Å. The observed polar surface area (51.81-62.23A^2) and stable solvent access area (98.63-237.64A^2) revealed the stability of the inhibitor inside the binding pocket. Less variation in the molecular surface area of 378.24-390.64A^2 during the simulation suggests that diosgenin is stable throughout the MD simulation.

1TQF (β-secretase) - Pterostilbene simulation

The solvated system comprises 13,465 water molecules and 46,292 atoms. After analysis of trajectory frames, the RMSDs for the Cα, backbone, and ligand fit protein were found to be between 1.23 and 2.18, 1.29 and 2.25, and 0.71 and 2.25 Å, respectively. During the equilibrium phase, the RMSDs of the Cα and backbone inhibitor combination increased until 62 ns, and then converged at 68 ns. Following equilibration, the RMSD of Cα atoms stabilized in the 2.18–1.622Å range during 62–100 ns (Figure 5d). The RMSF (Figure 7d) reveals changes in the Cα, B factor, and backbone of crucial binding amino acid residues inside the catalytic site showing fluctuations with RMSF values in the range of 0.45-3.71, 0.48-4.21, and 0.41-1.72Å, respectively. A low degree of protein structural flexibility was indicated by the fact that the selected protein inhibitor complex's Cα and backbone atoms' radius of rGyr remained stable throughout the MD simulation. Additionally, it is hypothesized that increased conformational relaxation in the protein-inhibitor complex is a consequence of the solvency effect (stabilization). Throughout the simulation, the ligand RMSD showed conformational changes stabilizing at 68 ns. The binding pocket residue RMSD, which shows a strong correlation with inhibitor movement, is also shown in Figure 5d. Hydrogen bonds were formed with Tyr68-Tyr71, Tyr71-Thr72, Thr231-Thr232, Thr232-Asn233, and Ile324-Ser325. The other interacting residues Leu30, Asp106, Phe108, Trp115, Arg235, Ile110, Ile118, Arg235,

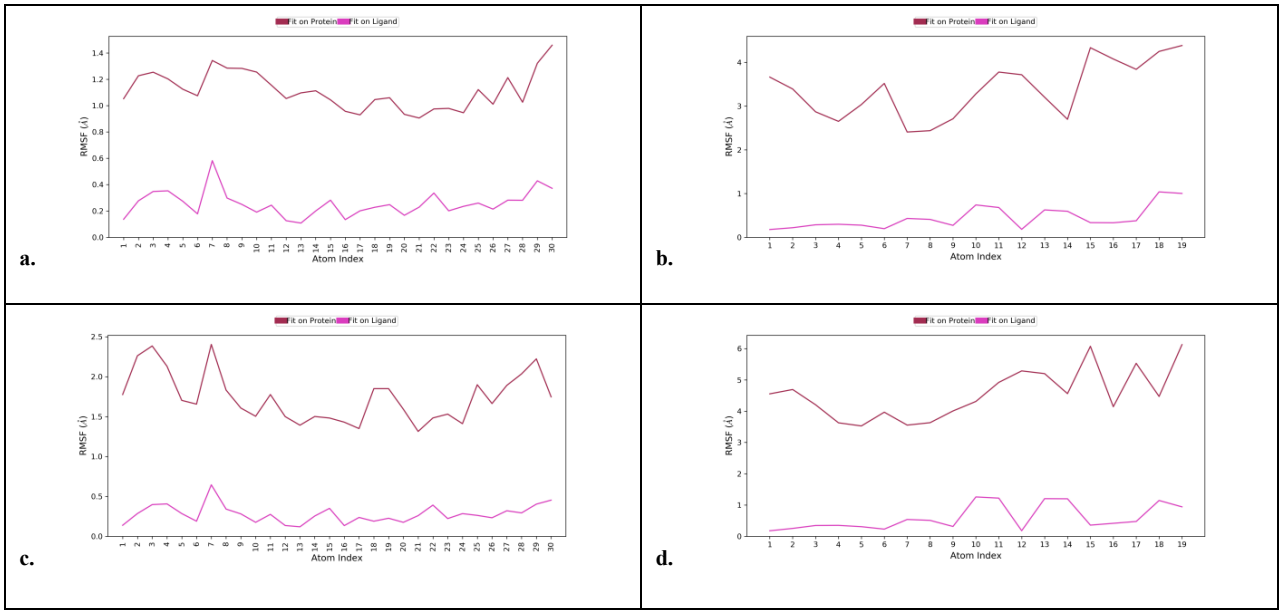

Figure 7. Root means square fluctuations (RMSF) of diosgenin and pterostilbene with Glycogen synthetase kinase beta (GSK-3β) and β-secretase. a. Plot showing the "RMSF of diosgenin fit on protein" for GSK-3β. b. Plot showing the "RMSF of pterostilbene fit on protein" for GSK-3β. c. A plot for β-secretase that shows the "RMSF of diosgenin fit on protein". d. Plot showing "RMSF of pterostilbene fit on protein" for β-secretase.

and Lys321 exhibited low RMSF values. As predicted from the XP docking interactions, similar binding interactions were demonstrated by the MD simulation trajectory analysis. The 3-methoxy group of the second phenyl ring of pterostilbene showed a hydrogen bond with the negatively charged Asp228 residue through a water molecule. These interactions occurred over 30% of the simulation duration in the chosen trajectory over the first 100 ns (Figure 6d). It also exhibited key hydrophobic interactions with Leu30, Tyr71, Phe108, Ile110, Trp115, Ile118, Arg235, and Lys321. The moderate conformational flexibility of Gln12, Asp106, Arg235, Leu263, Lys321, and Gln326 carried out the hydrogen bonding interaction at irregular frequencies. Additionally, pterostilbene/1TQF's clustered structure was produced using the trajectory clustering molecule after 100 frames, which were taken from simulation trajectory data (Schrodinger 2019-2). Pterostilbene demonstrated an average RMSD of 0.62Å and an average radius of gyration of 4.19Å following 62 ns of MD study. The polar surface area of 75.72-85.80A^2 and stable solvent access area of 60.34-320.21A^2 demonstrated the stability of the inhibitor inside the binding pocket. The stability of pterostilbene during MD simulation was indicated by less variations in the molecular surface area of 66.51-73.56A^2 during the simulation period.

Binding free energy - MMGBSA approach

The thermal binding free energy (ΔGbind) was calculated using the module thermal_mmgbsa.py Script for 102 trajectory frames over 100 ns. ΔGbind remained constant throughout the course of the MD simulation for all the protein complexes. The major contributors to ΔGbind were identified to be the van der Waals energy (ΔGvdW), lipophilic energy (ΔGlipo), and hydrogen bond energy (ΔGhbond) with moderate favorable Coulomb energy (ΔGcou) favoring the inhibitor binding, with the covalent energy (ΔGcov) and solvation energy (ΔGsolv) strongly disfavoring the inhibitor binding. The MMGBSA approach binding energy calculations are represented in Table 2 and Table 3. The binding free energy value, determined using the MM-GBSA technique, and the binding free energies obtained through docking, were in agreement with each other.

Drug-likeness and ADMET analysis

Selected ligands' SMILES uploaded to the web server assessed various parameters. The study of drug-like properties speeded up the drug research and development process. Table 4 shows the results of applying the Lipinski rule of five, the Ghose rule of filter, the Veber rule, the Egan rule, and the Muegge (LGVEM) rule to diosgenin and pterostilbene. To ascertain the bioactive function of a potent drug, these criteria have their own set of regulations. Both the compounds used in this study strictly adhered to the LGVEM rules and committed no violations.

Discussion

Studies reveal the pathophysiological role of β-amyloid and phosphorylated tau causing oxidative stress and inducing inflammatory pathways through releasing IL-6, TNF-α, and IL-1β in diabetes-associated AD. Despite the failure of many drugs during clinical trials as inhibitors of GSK-3β and β-secretase, therapeutic strategies to introduce lead candidates with this mechanism are encouraging due to their significant role in pathophysiological mechanism of the disease (30). However, a more novel approach of

Table 2. Binding free energies (in kcal/mol) of Diosgenin in complex with various proteins

Proteins	ΔGbind (Binding energy)	ΔGcou (Coulomb energy)	ΔGh-bond (Hydrogen bond energy)	ΔGlipo (Lipophilic energy)	ΔGvdw (Van der Waals energy)	ΔGCov (Covalent energy)	ΔGsolv (Solvation energy)
1J1B	-37.30	-32.81	0.35	-20.54	-37.16	-4.23	56.48
1TQF	-32.70	-53.92	5.61	-10.00	-3.15	-8.54	36.42
6IYC	-26.6	35.23	9.27	-14.14	-28.62	-24.08	-12.85
1ALU	-33.23	19.81	-2.50	-11.02	-35.44	4.74	-12.37
5M2J	-34.91	3.57	-19.94	-0.47	-41.18	13.91	9.30

Table 3. Binding free energies (in kcal/mol) of Pterostilbene in complex with various proteins

Proteins	ΔGbind (Binding energy)	ΔGcou (Coulomb energy)	ΔGh-bond (Hydrogen bond energy)	ΔGlipo (Lipophilic energy)	ΔGvdw (Van der Waals energy)	ΔGCov (Covalent energy)	ΔGsolv (Solvation energy)
1J1B	-27.48	-30.54	0.80	-15.77	-23.24	-3.41	46.77
1TQF	-13.59	-3.82	8.78	-5.24	10.41	-8.54	36.42
6IYC	53.13	166.89	25.33	-2.25	-17.94	-52.46	-80.14
1ALU	-20.27	5.20	-2.09	-8.53	-24.21	-2.10	8.80
5M2J	-49.05	-28.69	-18.71	-2.44	-30.62	11.56	21.06

Table 4. Molecular, pharmacokinetic, and ADMET (Absorption, distribution, metabolism, excretion, and toxicity) properties of diosgenin and pterostilbene

Parameter	Diosgenin	Pterostilbene
Molecular weight (gm/mol)	414.62	256.30
Hydrogen bond acceptor	3	3
Hydrogen bond donor	1	1
Log Po/w (Octanol-water partition coefficient)	4.45	3.02
Log S (Solubility)	-5.98	-4-01
Topological polar surface area (A2)	38.69	38.69
Gastrointestinal absorption	High	High
Blood brain barrier permeation	Yes	Yes
Log Kp (Plasma partition coefficient)	-4.80 cm/s	-5.18 cm/s
Lipinski rule	Yes; 1 violation	Yes
Ghose rule	No; 2 violations	Yes
Veber rule	Yes	Yes
Egan rule	No; 1 violation	Yes
Bioavailability	0.55	0.55
P-glycoprotein substrate	No	No
CYP3A4 inhibitor	No	No

targeting multiple receptors is being focused against a single target approach for complex neurological diseases like AD. In brief, molecular docking in conjunction with simulation studies and pharmacokinetic analysis was applied to meet the critical challenges faced in designing efficient multi-target drugs to treat AD. Initially, the phytoconstituents diosgenin and pterostilbene were docked with GSK-3β, β-secretase, γ-secretase, TNF-α, and IL-6 using the most widely accepted docking program, Schrödinger, and then the docked complexes with good binding characteristics were selected for simulation studies. Also, the binding energies were calculated to confirm their binding modes. Key residues in each target were identified and compared with standard inhibitors. GSK-3β, which is an enzyme responsible for tau phosphorylation, is considered an important target in the treatment of AD. The docked complex of diosgenin with GSK-3β revealed interactions with Thr138 and Gln185, which play a role in complex binding stabilization (31). The hinge residue interactions seen with pterostilbene are considered crucial for molecular recognition, as reported with most GSK-3β inhibitors (32). The docking scores of diosgenin and pterostilbene with GSK-3β were highly comparable to those of Tideglusib, a recent GSK-3β inhibitor that failed in phase II studies and had a docking score of 11.37 kcal/mol (33).

β-secretase is another essential enzyme associated with the processing of the β- amyloid precursor protein, involved in the amyloidogenic pathway. Its inhibition improves cognition as it blocks the process that generates

amyloid plaques. With this target, the ligands diosgenin and pterostilbene showed several interactions in the S2 subpocket, representing an essential feature for binding to it (34). One of the hydrogen bonds formed by pterostilbene's methoxy group with Asp32 in the S1 pocket is significant for catalytic activity, as Asp32 is one of the two catalytically active aspartates located in the center of the active site reported in most inhibitors. (35,36).

The docking scores of diosgenin and pterostilbene with β-secretase were found to be very close to those of Atabecestat, a standard β-secretase inhibitor with a docking score of -8.0 kcal/mol (37). γ-Secretase, which is also involved in the amyloid precursor protein processing, when docked with diosgenin and pterostilbene, showed docking activity similar to the standard γ-secretase inhibitor L-685458 with a docking score of −10.19 kcal/mol (38). Upon docking the two phytoconstituents with the anti-inflammatory targets IL-6 and TNF-α, many hydrogen bonds were revealed, which were crucial for their binding-induced inhibition. Thus, these interactions between the ligands indicated their ability to modulate the inflammatory mechanisms to provide neuroprotection. Simulation studies of the ligands with the targets GSK-3β and β-secretase demonstrated a highly stable solvent surface area, confirming the stability of the inhibitor inside the binding pocket, and fewer variations in the molecular surface area, indicating the stability of the bound complex.

Although the compounds exhibited good binding affinities towards the targets, it does not mean they possess the required absorption, distribution, metabolism, and excretion (ADME) properties for good bioavailability. Drug pharmacokinetics, commonly referred to as absorption, distribution, metabolism, and excretion is the study of how drugs enter, pass through, and exit the body (39). Therefore, as the study of drug-like properties speeds up the drug research and development process, pharmacokinetic analysis of the ligands was also carried out. The analysis was conducted using the web tool SwissADME.

The major characteristics assessed included molecular weight (MW), topological polar surface area (TPSA), solubility (Log S), consensus estimated logP, and predicted bioavailability. The ligands confirmed their good pharmacokinetic characteristics, as indicated by their bioavailability score of 0.55. Additionally, they exhibit promising CNS action with a TPSA of less than 40 Å2. Although the compounds were moderately soluble in water, they showed increased blood-brain barrier permeability and gastrointestinal absorption, which are significant for drugs that treat AD.

Both the compounds used in this study strictly adhered to the LGVEM rules and committed no violations. This illustrates the potential for these compounds to be used as medications. Reducing tau phosphorylation and amyloid plaques is the most desirable strategy; however, the failure of the inhibitors in phase II trials also focused the research toward alternative neuroinflammatory pathways to curb the disease progression (40).

Conclusion

In this study, the selected ligands diosgenin and pterostilbene were docked with pharmacologically relevant targets associated with diabetes and AD. This study provided evidence for the mechanism of interaction of the ligands with multiple targets, which might prove beneficial in treating diabetes-associated Alzheimer's disease. However, *in vitro* and *in vivo* studies are recommended for further validation of the combined action of the ligands. Encouraging results and theoretical predictions confirmed the precise mechanisms targeting the direct and alternative pathways that paved the way for novel treatments. The *in silico* approaches might be effective in reducing research costs by quickly confirming mechanisms through computerized tools within a very short time. The study findings collectively illustrate the novelty of diosgenin and pterostilbene as potential drug candidates in AD therapy.

Acknowledgments

The authors are thankful to Anurag University for providing relevant software to do the research work.

Authors' Contribution

Conceptualization: Syeda Jabeen Fatima.
Investigation: Syeda Jabeen Fatima.
Methodology: Syeda Jabeen Fatima.
Project administration: Devarakonda Krishna Prasad and Syeda Jabeen Fatima.
Software: Syeda Jabeen Fatima.
Supervision: Devarakonda Krishna Prasad.
Validation: Devarakonda Krishna Prasad and Syeda Jabeen Fatima.
Writing-original draft: Syeda Jabeen Fatima.
Writing-review & editing: Syeda Jabeen Fatima and Devarakonda Krishna Prasad.

Conflict of interests

The authors declare no conflict of interest.

Ethical considerations

The manuscript has been reviewed for plagiarism, and the authors took into account all ethical considerations, including duplication.

Funding/Support

The authors declare that they have not received any financial support.

References

1. Mahmoudi N, Kiasalari Z, Rahmani T, Sanaierad A, Afshin-Majd S, Naderi G, et al. Diosgenin attenuates cognitive impairment in streptozotocin-induced diabetic

rats: underlying mechanisms. Neuropsychobiology. 2021;80(1):25-35. doi: 10.1159/000507398.
2. Cao Q, Tan CC, Xu W, Hu H, Cao XP, Dong Q, et al. The prevalence of dementia: a systematic review and meta-analysis. J Alzheimers Dis. 2020;73(3):1157-66. doi: 10.3233/jad-191092.
3. Rana K, Gautam P. A review on antioxidants as therapeutic in use of oxidative stress and neurodegenerative disease. Int J Pharm Qual Assur. 2022;13(1):77-82. doi: 10.25258/ijpqa.13.1.16.
4. Sebastian MJ, Khan SK, Pappachan JM, Jeeyavudeen MS. Diabetes and cognitive function: an evidence-based current perspective. World J Diabetes. 2023;14(2):92-109. doi: 10.4239/wjd.v14.i2.92.
5. Chen GF, Xu TH, Yan Y, Zhou YR, Jiang Y, Melcher K, et al. Amyloid beta: structure, biology and structure-based therapeutic development. Acta Pharmacol. Sin. 2017;38(9):1205-35.
6. Bachurin SO, Bovina EV, Ustyugov AA. Drugs in clinical trials for Alzheimer's disease: the major trends. Med Res Rev. 2017;37(5):1186-225. doi: 10.1002/med.21434.
7. Najem D, Bamji-Mirza M, Chang N, Liu QY, Zhang W. Insulin resistance, neuroinflammation, and Alzheimer's disease. Rev Neurosci. 2014;25(4):509-25. doi: 10.1515/revneuro-2013-0050.
8. Makhoba XH, Viegas C Jr, Mosa RA, Viegas FP, Pooe OJ. Potential impact of the multi-target drug approach in the treatment of some complex diseases. Drug Des Devel Ther. 2020;14:3235-49. doi: 10.2147/dddt.s257494.
9. Athar T, Al Balushi K, Khan SA. Recent advances on drug development and emerging therapeutic agents for Alzheimer's disease. Mol Biol Rep. 2021;48(7):5629-45. doi: 10.1007/s11033-021-06512-9.
10. Samtiya M, Aluko RE, Dhewa T, Moreno-Rojas JM. Potential health benefits of plant food-derived bioactive components: an overview. Foods. 2021;10(4):839. doi: 10.3390/foods10040839.
11. Raghav SS, Kumar B, Sethiya NK, Kaul A. A mechanistic insight on phytoconstituents delivering hypoglycemic activity: a comprehensive overview. Future Pharmacol. 2022;2(4):511-46. doi: 10.3390/futurepharmacol2040032.
12. Upadhyay P, Sadhu A, Singh PK, Agrawal A, Ilango K, Purohit S, et al. Revalidation of the neuroprotective effects of a United States patented polyherbal formulation on scopolamine induced learning and memory impairment in rats. Biomed Pharmacother. 2018;97:1046-52. doi: 10.1016/j.biopha.2017.11.008.
13. Lin WS, Leland JV, Ho CT, Pan MH. Occurrence, bioavailability, anti-inflammatory, and anticancer effects of pterostilbene. J Agric Food Chem. 2020;68(46):12788-99. doi: 10.1021/acs.jafc.9b07860.
14. Meng J, Chen Y, Bi F, Li H, Chang C, Liu W. Pterostilbene attenuates amyloid-β induced neurotoxicity with regulating PDE4A-CREB-BDNF pathway. Am J Transl Res. 2019;11(10):6356-69.
15. Sidhu JS, Sharma S, Singh A, Garg N, Kaur N, Singh N. A naphthalimide-based novel "Turn-On" fluorescence approach for the determination of uric acid and monitoring of xanthine oxidase activity. Anal Methods. 2019;11(32):4190-6. doi: 10.1039/c9ay01464k.
16. Jacobson MP, Pincus DL, Rapp CS, Day TJ, Honig B, Shaw DE, et al. A hierarchical approach to all-atom protein loop prediction. Proteins. 2004;55(2):351-67. doi: 10.1002/prot.10613.
17. Roos K, Wu C, Damm W, Reboul M, Stevenson JM, Lu C, et al. OPLS3e: extending force field coverage for drug-like small molecules. J Chem Theory Comput. 2019;15(3):1863-74. doi: 10.1021/acs.jctc.8b01026.
18. Friesner RA, Murphy RB, Repasky MP, Frye LL, Greenwood JR, Halgren TA, et al. Extra precision glide: docking and scoring incorporating a model of hydrophobic enclosure for protein-ligand complexes. J Med Chem. 2006;49(21):6177-96. doi: 10.1021/jm051256o.
19. Guo Z, Mohanty U, Noehre J, Sawyer TK, Sherman W, Krilov G. Probing the alpha-helical structural stability of stapled p53 peptides: molecular dynamics simulations and analysis. Chem Biol Drug Des. 2010;75(4):348-59. doi: 10.1111/j.1747-0285.2010.00951.x.
20. Essmann U, Perera L, Berkowitz ML, Darden T, Lee H, Pedersen LG. A smooth particle mesh Ewald method. J Chem Phys. 1995;103(19):8577-93. doi: 10.1063/1.470117.
21. Martyna GJ, Klein ML, Tuckerman M. Nosé-Hoover chains: the canonical ensemble via continuous dynamics. J Chem Phys. 1992;97(4):2635-43. doi: 10.1063/1.463940.
22. Martyna GJ, Tobias DJ, Klein ML. Constant pressure molecular dynamics algorithms. J Chem Phys. 1994;101(5):4177-89. doi: 10.1063/1.467468.
23. Tuckerman M, Berne BJ, Martyna GJ. Reversible multiple time scale molecular dynamics. J Chem Phys. 1992;97(3):1990-2001. doi: 10.1063/1.463137.
24. Akkus E, Tayfuroglu O, Yildiz M, Kocak A. Accurate binding free energy method from end-state MD simulations. J Chem Inf Model. 2022;62(17):4095-106. doi: 10.1021/acs.jcim.2c00601.
25. Daina A, Michielin O, Zoete V. SwissADME: a free web tool to evaluate pharmacokinetics, drug-likeness and medicinal chemistry friendliness of small molecules. Sci Rep. 2017;7:42717. doi: 10.1038/srep42717.
26. Ghose AK, Viswanadhan VN, Wendoloski JJ. A knowledge-based approach in designing combinatorial or medicinal chemistry libraries for drug discovery. 1. A qualitative and quantitative characterization of known drug databases. J Comb Chem. 1999;1(1):55-68. doi: 10.1021/cc9800071.
27. Veber DF, Johnson SR, Cheng HY, Smith BR, Ward KW, Kopple KD. Molecular properties that influence the oral bioavailability of drug candidates. J Med Chem. 2002;45(12):2615-23. doi: 10.1021/jm020017n.
28. Muegge I, Heald SL, Brittelli D. Simple selection criteria for drug-like chemical matter. J Med Chem. 2001;44(12):1841-6. doi: 10.1021/jm015507e.
29. Mortuza MG, Roni MA, Kumer A, Biswas S, Saleh MA, Islam S, et al. A computational study on selected alkaloids as SARS-CoV-2 inhibitors: PASS prediction, molecular docking, ADMET analysis, DFT, and molecular dynamics simulations. Biochem Res Int. 2023;2023:9975275. doi: 10.1155/2023/9975275.
30. Llorens-Martín M, Jurado J, Hernández F, Avila J. GSK-3β, a pivotal kinase in Alzheimer disease. Front Mol Neurosci. 2014;7:46. doi: 10.3389/fnmol.2014.00046.
31. Arfeen M, Bharatam PV. Design of glycogen synthase kinase-3 inhibitors: an overview on recent advancements. Curr Pharm Des. 2013;19(26):4755-75. doi:

10.2174/1381612811319260007.
32. Ilouz R, Kowalsman N, Eisenstein M, Eldar-Finkelman H. Identification of novel glycogen synthase kinase-3beta substrate-interacting residues suggests a common mechanism for substrate recognition. J Biol Chem. 2006;281(41):30621-30. doi: 10.1074/jbc.M604633200.
33. Wondie ML. Recent advances in the treatment of Alzheimer's disease: current overview and future prospects. Retrieved from: https://archive.interconf.center/index.php/conference-proceeding/article/view/5093.
34. Yu Z, Wu S, Zhao W, Ding L, Shiuan D, Zheng F, et al. Biological evaluation and interaction mechanism of beta-site APP cleaving enzyme 1 inhibitory pentapeptide from egg albumin. Food Sci Hum Wellness. 2020;9(2):162-7. doi: 10.1016/j.fshw.2020.01.004.
35. Cosconati S, Marinelli L, Di Leva FS, La Pietra V, De Simone A, Mancini F, et al. Protein flexibility in virtual screening: the BACE-1 case study. J Chem Inf Model. 2012;52(10):2697-704. doi: 10.1021/ci300390h.
36. Koriyama Y, Hori A, Ito H, Yonezawa S, Baba Y, Tanimoto N, et al. Discovery of atabecestat (JNJ-54861911): a thiazine-based β-amyloid precursor protein cleaving enzyme 1 inhibitor advanced to the phase 2b/3 EARLY clinical trial. J Med Chem. 2021;64(4):1873-88. doi: 10.1021/acs.jmedchem.0c01917.
37. Niu Y, Ma C, Jin H, Xu F, Gao H, Liu P, et al. The discovery of novel β-secretase inhibitors: pharmacophore modeling, virtual screening, and docking studies. Chem Biol Drug Des. 2012;79(6):972-80. doi: 10.1111/j.1747-0285.2012.01367.x.
38. Zhou R, Yang G, Guo X, Zhou Q, Lei J, Shi Y. Recognition of the amyloid precursor protein by human γ-secretase. Science. 2019;363(6428):eaaw0930. doi: 10.1126/science.aaw0930.
39. Pires DE, Blundell TL, Ascher DB. pkCSM: predicting small-molecule pharmacokinetic and toxicity properties using graph-based signatures. J Med Chem. 2015;58(9):4066-72. doi: 10.1021/acs.jmedchem.5b00104.
40. Bandaru LJ, Murumulla L, Bindu Lasya C, Krishna Prasad D, Challa S. Exposure of combination of environmental pollutant, lead (Pb) and β-amyloid peptides causes mitochondrial dysfunction and oxidative stress in human neuronal cells. J Bioenerg Biomembr. 2023;55(1):79-89. doi: 10.1007/s10863-023-09956-9.